



**HAL**  
open science

## Are average speed emission functions scale-free?

Delphine Lejri, Ludovic Leclercq

► **To cite this version:**

Delphine Lejri, Ludovic Leclercq. Are average speed emission functions scale-free?. Atmospheric Environment, 2020, 224, 12p. 10.1016/j.atmosenv.2020.117324 . hal-02487633v2

**HAL Id: hal-02487633**

**<https://hal.science/hal-02487633v2>**

Submitted on 24 Mar 2020

**HAL** is a multi-disciplinary open access archive for the deposit and dissemination of scientific research documents, whether they are published or not. The documents may come from teaching and research institutions in France or abroad, or from public or private research centers.

L'archive ouverte pluridisciplinaire **HAL**, est destinée au dépôt et à la diffusion de documents scientifiques de niveau recherche, publiés ou non, émanant des établissements d'enseignement et de recherche français ou étrangers, des laboratoires publics ou privés.

# 1 **Are average speed emission functions scale-free?**

2 D. Lejri, L. Leclercq

3  
4 Univ. Gustave Eiffel, Univ. Lyon, ENTPE, LICIT, Lyon, France

## 6 **Abstract**

7  
8 Although emission models have been designed using vehicle data over driving cycles of a few  
9 minutes, they are often applied at large scale to estimate total emission (inventories). In between,  
10 there is a range of scales in use in traffic and environmental studies (road sections, sub-areas,  
11 etc.). Coupling a traffic microsimulation with COPERT emission factors at different scales reveals  
12 scaling biases. We compare network fuel consumption (FC) and nitrogen oxide (NO<sub>x</sub>) emissions  
13 resulting from emission calculations based on different spatial decompositions. The results show  
14 that for an area of Paris covering 3 km<sup>2</sup>, the differences due to the aggregation scale for emissions  
15 range from 5 to 17% depending on the pollutant, spatial partitioning and traffic conditions. These  
16 discrepancies can be reduced using a distance-weighted mean speed, which is not a scale-  
17 consistent definition of mean travel speed. They can almost be cancelled by using a correction  
18 term derived analytically in this paper, thus consistency can be guaranteed between emissions  
19 assessed at different scales. Finally, a case study shows that it is possible to evaluate FC and NO<sub>x</sub>  
20 emissions on a large-scale network from a sample of traffic data (probes), and obtain the  
21 corrective term to be applied to remove scaling bias. The most critical step is the accurate  
22 estimation of the total travel distance. The gaps were successfully reduced to a maximum of 8%  
23 in congestion for a penetration rate of about 20%.

24 **Keywords:** Average speed model, emission factors, COPERT, scale consistency, driving cycle, mean  
25 speed.

## 27 **Highlights**

- 28 • Highlighting the scaling inconsistency of emission laws due to the definition of mean speed
- 29 • A corrective term is derived to estimate the biases of different aggregation scales
- 30 • Floating car data is simulated to estimate unbiased global emissions

## 32 1. Introduction

33

34 Road traffic is a major source of air quality deterioration in large cities. Despite the advances made  
35 in vehicle technologies and traffic management policies, travel needs are increasing and the road  
36 sector remains a major contributor to air pollution, with significant effects on public health. These  
37 effects on both health and climate change are well established (EEA, 2017; WHO, 2013). Policy-  
38 makers are looking for solutions to reduce greenhouse gases and pollutant emissions. To this end,  
39 efforts in recent years have focused on the rigorous assessment of emission reduction measures  
40 (Fontes et al., 2015; York Bigazzi and Rouleau, 2017).

41

42 The challenging issue is therefore to produce a robust "traffic-emission" modeling chain and  
43 assess the corresponding uncertainties (Fallah Shorshani et al., 2015). In particular, in urban  
44 areas, periods of congestion contribute significantly to fuel consumption and pollutant emissions,  
45 which is why traffic dynamics should be estimated accurately (Lejri et al., 2018). Traffic  
46 microsimulators are typically used to provide relevant traffic data for emission calculations.

47

48 Another issue to be addressed is the way emissions are calculated. Initially, the microscopic scale,  
49 which provides the most detailed information seems to be the most appropriate. Indeed micro-  
50 emission models such as CMEM (Barth et al., 2001), PHEM (Zallinger, 2009) and CRUISE (AVL,  
51 2018), provide instantaneous consumption and emission data from vehicle trajectories measured  
52 or supplied by a microscopic traffic simulator. On a large urban scale, this modeling chain is time  
53 and data consuming; moreover, it does not guarantee an experimentally validated evaluation of  
54 emissions.

55

56 Consequently, aggregate emission models are widely used for the environmental assessment of  
57 traffic-related emissions. Macroscopic emission models such as COPERT (Ntziachristos et al.,  
58 2009) and HBEFA (Hausberger et al., 2009) require only two traffic variables as inputs: a  
59 description of the mean travel speed of the vehicle flow and the corresponding travel distance.  
60 Moreover, the COPERT model has shown that it is capable of integrating traffic dynamics and  
61 particularly the effects of congestion through average speed or a derived indicator (speed  
62 distribution)(Lejri et al., 2018; Samaras et al., 2017). The accuracy of emissions in fact depends  
63 on the accuracy of traffic variables estimates.

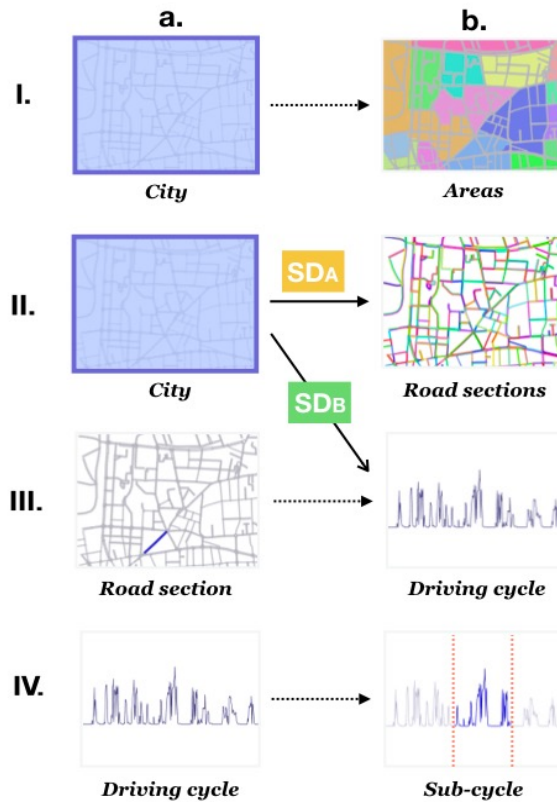
64

65 In this paper, we focus on the COPERT aggregate emission model, which is usually applied at  
66 different scales. This macroscopic model is mainly applied at a large urban scale to carry out  
67 emission inventories. In this case, highly aggregated traffic variables (i.e. total travel distance and  
68 a uniform mean travel speed over the whole city) are used to estimate traffic conditions. In order  
69 to estimate emissions more locally, the city can be divided into several sub-areas characterized  
70 by different traffic conditions. In this case, the related emissions are then evaluated separately for  
71 each sub-area. More recently, given the growing impact of congestion on emissions, COPERT has  
72 also been used at the link level (road sections)(Borge et al., 2012; Christos Samaras et al., 2014).  
73 In this case, the traffic variables should be specifically estimated for each link in order to derive  
74 the corresponding emissions. Finally, with more probe and GPS data available, the question of  
75 applying COPERT to a vehicle fleet arises. This last scale is used to estimate the average emissions  
76 over a trip, which is the closest to the design of the model. Indeed, the emission laws are  
77 established on the basis of measurements made over specific driving cycles, including the  
78 ARTEMIS database (André, 2004; Boulter and McCrae, 2007). The set of cycles corresponding to  
79 traffic conditions in dense urban areas has the following characteristics: a duration of 5min, a  
80 length of 6km, an average speed of 22km/h and a speed standard deviation of around 14km/h.

81

82 As noted, to perform emission calculations, spatial decompositions are often used. At all these  
83 scales, the results obtained from COPERT are usually considered valid as soon as mean speed and  
84 travel distance are deemed accurate. In terms of emissions, the relation between the scales is

85 obvious: emissions are additive. Then, to move from a smaller to a larger scale, sub-area emissions  
 86 simply need to be added together to obtain the overall emission.  
 87 However, it is well known in traffic theory that mean travel speed, the variable at the center of the  
 88 emission calculations, is not easily transferable from one spatial partitioning to larger one. Mean  
 89 travel speed is the ratio of travel distance over travel time, which are also both additive variables.  
 90 But, the mean travel speed of an area is neither the sum, nor the average of the sub-areas mean  
 91 travel speeds. Therefore, the following questions arise: Could emission laws based on a non-  
 92 scalable variable, provide scale-consistent results? Are COPERT emission calculations consistent  
 93 from one spatial partitioning to another?  
 94



95  
 96  
 97 **Figure 1 Various spatial decompositions for emission calculations**

98  
 99 This work seeks to highlight the discrepancies observed in terms of emissions for different spatial  
 100 decompositions. Four examples of frequent spatial decompositions in emission calculations are  
 101 shown in Figure 1. What are the differences on overall emissions between a calculation at a city  
 102 scale (IIa.) and at link level (IIb.)? This paper points out biases induced by mean speed emission  
 103 functions when emission calculation scales are different. It focuses on COPERT emission laws, but  
 104 the issue of scale-inconsistency occurs more generally for any model that uses either non scalable  
 105 variables, e.g. mean speed, or non-linear emission functions.  
 106

107 The article is organized as follows. The issue is first stated for theoretical and measured driving  
 108 cycles (section 3). Then, fuel consumptions (FC) and nitrogen oxide (NOx) emission scaling biases  
 109 are evaluated for the 6<sup>th</sup> district of Paris (see section 4). This case study focuses on a dynamic  
 110 traffic microsimulation, which is used to calculate emissions according to different spatial  
 111 decompositions (individual road sections and individual vehicles). Traffic microsimulation  
 112 provides all vehicle trajectories. This detailed information is convenient for performing all  
 113 possible aggregations and then comparative analyses. After highlighting the scaling bias  
 114 associated with the emission calculations and proposing a method for reducing it, we focus on a

115 practical case for real application (see section 5). The issue addressed here is to evaluate network  
 116 emissions with only partial local traffic data. We show how it is possible to achieve network  
 117 emissions consistent with local scale from a sample of probe vehicles (e.g. GPS data). The paper  
 118 ends with a conclusion (section 6) and a discussion (section 7).

119  
 120

## 121 2. Material

122

123 This section is devoted to analyzing the way emissions are calculated using COPERT emission  
 124 functions, depending on the spatial partitioning chosen. We first propose an overview of mean  
 125 speed definitions in order to facilitate understanding of the following paragraphs and then recall  
 126 how average speed is involved in the emission calculations.

127

### 128 2.1. Mean speed flow

129

130 In traffic theory, it is known that the mean speed of the vehicle flow is not transferable from one  
 131 spatial decomposition to another. Basically, this means that the mean speed for a set of vehicles is  
 132 not the average of the mean speed per vehicle, similarly the mean speed for an aggregate of sub-  
 133 regions is not the average of the mean speed per region. A proper calculation of the mean speed  
 134 requires the estimation of related travel distance and travel time. These variables are both  
 135 additive and can be easily transferred from one scale to another.

136

137 Let us consider a region  $[r, r+\Delta r]$  with  $n$  vehicles. Each vehicle  $j$  ( $j=1\dots n$ ) is travelling a distance  $d_j$   
 138 and stays  $\tau_j$  in this region during a given interval  $[t; t+\Delta t]$ . An empirical definition of the spatial  
 139 mean speed in the region of the space-time diagram of size  $\Delta t \Delta r$  is given by (Edie, 1965). It is  
 140 relevant when  $\Delta t$  and  $\Delta r$  are large.

141

$$142 \quad V = \frac{\sum_{j=1}^n d_j}{\sum_{j=1}^n \tau_j} \quad (1)$$

143

144 In the next sections, the space-time regions explored are, for example, the network road sections  
 145 and 6min time periods. By introducing the vehicular mean speed  $v_j$ , formula (1) becomes  $V =$   
 146  $\sum(\tau_j v_j) / \sum \tau_j$ , that is why the spatial mean speed can be considered as the time-weighted average  
 147 of vehicle mean speeds, and will therefore be noted  $V_t$ . This spatial mean speed definition  
 148 (Lagrangian approach) includes all vehicle entries and exits in the study region, and captures all  
 149 the dynamics of the vehicles (Lejri et al., 2018). This is the speed relevant for estimating emissions.  
 150 However, other definitions exist and will be explored later (section 3.2). The most common is the  
 151 distance-weighted average of vehicle mean speeds (noted  $V_d$ ), also named punctual mean speed.  
 152 It corresponds to observations made at a point in the road section (Eulerian approach), that is  
 153 why it cannot capture all the dynamics of the vehicles. Therefore, it is not a suitable choice for  
 154 calculating emissions.

155 Similarly, when considering a region decomposed in  $m$  sub-areas, the mean speed  $V$  of the whole  
 156 region is related to the total travel distance  $d_i$  and the total travel time  $\tau_i$  of the sub-areas ( $i=1\dots m$ ).  
 157 Spatial and punctual global mean speed are defined as the time- and distance-weighted average  
 158 of sub-area mean speeds  $v_i$ .

159 Both these definitions are linked together by the Wardrop formula (Wardrop, 1952):

$$160 \quad V_d = V_t + \frac{\sigma_t^2}{V_t}, \text{ with } \sigma_t^2 = \frac{1}{\sum \tau_i} \sum \tau_i (v_i - V_t)^2 \quad (2)$$

161

162 Whatever the spatial decomposition considered, when it comes to characterizing a region mean  
 163 speed, the right definition is the time-weighted average of the sub-regions mean speeds  $V_t$ . In this  
 164 case, the vehicles' total travel distances and total travel times are properly aggregated at a higher  
 scale without any loss of information. On the other hand, the distance-weighted mean speed  $V_d$ ,

165 depends on the decomposition considered, as suggested in formula (2), since it depends on  $\sigma_t$ ,  
166 the time-weighted standard deviation of local speeds. This relationship has been verified using  
167 experimental data (Knoop et al., 2009). The way these mean speed definitions interact with  
168 emission calculations is highlighted in section 3.

169  
170

## 171 **2.2. COPERT construction**

172

173 COPERT IV has been widely used in most European Countries for compiling national emission  
174 inventories (EMEP/EEA, 2016), but it is also increasingly used for emission modeling at the street  
175 level (Borge et al., 2012).

176

177 This method relies on the fact that average emissions over a trip vary according to the average  
178 travel speed. Hot exhaust emissions have been examined on the basis of measurements in several  
179 research programs (COST319, FP4 MEET, FP6 ARTEMIS). These measurements were mainly  
180 conducted on a chassis dynamometer on which the test vehicle is run over a specific driving cycle  
181 while its emissions were collected and analyzed. The emission level was then associated with the  
182 mean travel speed over the cycle.

183 The driving cycle should represent real driving conditions and must therefore be carefully chosen.  
184 The New European Driving Cycle (NEDC), a synthetic type-approval driving cycle, has been  
185 replaced since 2017 by the World Harmonized Light Vehicles Test Procedures (WLTC), to  
186 overcome the shortcomings of the previous test procedure. The Common Artemis Driving Cycle  
187 (CAAdC) (André, 2004) has also been proposed as being more representative of the behavior of  
188 vehicles in real conditions (André and Rapone, 2009). All of these cycles are used to feed the  
189 European experimental database that has been developed and examined within the ERMES group  
190 for emission modeling.

191

192 The emission-average speed relationship is established by combining the results of tests using  
193 cycles with different average speeds. Unitary emission factors (EF) consist of continuous speed  
194 functions designed using regression analysis to associate the emission level per km with travel  
195 speed. These speed curves are drawn for each pollutant and each vehicle class (*e.g.* passenger cars,  
196 light duty vehicles, buses and heavy-duty vehicles) and technology (diesel or gasoline, Euro 1 to  
197 Euro 6).

198

199 To our knowledge, the emission factor values are not established for a unique length but on  
200 driving cycles with various characteristics (especially various lengths). This means that (i) mean  
201 emission laws integrate a potential internal bias related to multiple (and inconsistent) mean  
202 speed values being used, and that (ii) we are actually missing a clear reference scale (resolution  
203 at which the relationship between average speed and emission rates are established).

204 In (Papadopoulos et al., 2018), the authors describe how the resolution affects EF derived from  
205 PEMS data and finally propose to establish EF on the basis of a 500m resolution. It also highlights  
206 that the extensive use of PEMS data may lead to heterogeneous methodologies for developing EF.

## 207 **2.3. Using COPERT in the framework**

### 208 **2.4. of an evaluation**

209

210 Thus, the COPERT model is based on unit emission factors per vehicle and per km travelled. It is  
211 therefore possible to estimate the emissions of a vehicle trip knowing its mean travel speed and  
212 its travel distance. However, the methodology was designed to produce emission inventories, i.e.  
213 to assess emissions from a set of vehicles or trips. It therefore assumes that the relationship  
214 remains valid at the scale of a vehicle flow and that the determination of the average speed and  
215 the total distance travelled by these vehicles makes it possible to assess the associated emissions.

216 Defining the most appropriate scale for conducting an environmental assessment with COPERT is  
 217 a challenging issue. (C. Samaras et al., 2014) considers that segments in the order of 400 m provide  
 218 good spatial resolution to model emissions in a street network, in relation to the scale for  
 219 establishing EFs.

220  
 221 In practice, COPERT methodology is applied to various scales and can even be extended to  
 222 evaluating very large scales such as national inventories over a year. In this case, traffic conditions  
 223 (average speed) are characterized on a much larger scale than the driving cycle. However, behind  
 224 this average traffic situation lie very varied traffic conditions, characterized by different average  
 225 speeds. This is the case in dense urban conditions, where localized congestion phenomena occur.  
 226 Therefore, it seems appropriate to propose a spatial disaggregation, allowing a more detailed  
 227 description of traffic conditions (and associated emissions), even in case of monitoring network  
 228 emissions. Traffic simulations and measurements generally explore two different scales: the road  
 229 section level and the vehicle level (trajectories). Unlike the global scale, these local scales make it  
 230 possible to differentiate between streets or routes in terms of traffic and emissions.

231 However, if we do so, what will be the impact of spatial partitioning on the emissions? Are the  
 232 total emissions resulting from various spatial decompositions still consistent?  
 233

### 234 3. Problem statement

#### 235 3.1. Simple example

236  
 237 Although it is unusual to work at the vehicle scale with COPERT, it seems necessary to start from  
 238 the operating conditions of the bench measurements used to feed the model. This will help to  
 239 better highlight the key roleplayed by the speed definition.

240 For instance, if we consider a vehicle trip of distance  $D$  and divide it into two sub-trips of distances  
 241  $d_1$  and  $d_2$ , we can specify the total emission  $E_{tot}$  as the sum of sub-trip emissions  $e_1$  and  $e_2$ , because  
 242 the emissions are cumulative quantities. Knowing the mean speeds of (i) the total trip ( $V$ ) and (ii)  
 243 the two sub-trips ( $v_1$  and  $v_2$ ), these emissions can be assessed using the COPERT emission  
 244 function  $f$ .

$$245 \quad E_{tot} = e_1 + e_2$$

$$246 \quad D f(V) = d_1 f(v_1) + d_2 f(v_2) \quad (3)$$

247  
 248 Assuming that the emission function  $f$  can be approximated with a third order polynomial,  
 249 relation (3) becomes:

$$250 \quad a_1 DV + a_2 DV^2 + a_3 DV^3 = a_1(d_1 v_1 + d_2 v_2) + a_2(d_1 v_1^2 + d_2 v_2^2) + a_3(d_1 v_1^3 + d_2 v_2^3)$$

251 with  $f(v) \approx a_0 + a_1 v + a_2 v^2 + a_3 v^3$

252  
 253 Equality is verified if these three conditions are verified:

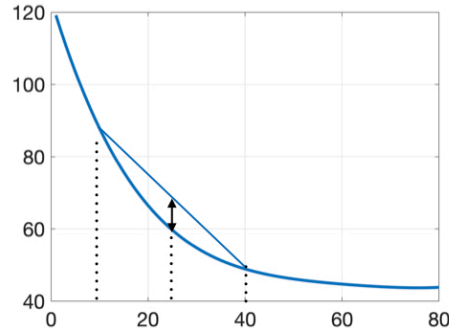
$$254 \quad \begin{cases} V = (d_1 v_1 + d_2 v_2)/D \\ 255 \quad V^2 = (d_1 v_1^2 + d_2 v_2^2)/D \\ 256 \quad V^3 = (d_1 v_1^3 + d_2 v_2^3)/D \end{cases}$$

257 In fact, these conditions cannot be verified simultaneously except if  $v_1 = v_2$ . This underlines the  
 258 fact that emissions are dependent on the spatial decomposition considered when calculating  
 259 them. It is directly related to the definition of emission functions. Indeed, COPERT emission  
 260 factors have been designed according to a traffic variable that is not transferable from one scale  
 261 to another: the average travel speed. This effect is enhanced by the convexity of emission function

262  $f$  (Fig. 2). Indeed, if  $f$  is convex, then  $f(\bar{X}) \leq \overline{f(X)}$ .

263

264 Also, the second conclusion that can be drawn is that defining the global mean speed as a distance-  
 265 weighted average (first condition) reduces the gap between the total trip emission and the sum  
 266 of sub-trip emissions, by cancelling one of the three terms. This result is interesting because it is  
 267 not the correct definition of the average speed of the trip, which is distance over time. But it is a  
 268 first step towards achieving consistency between the emission calculation scales.  
 269

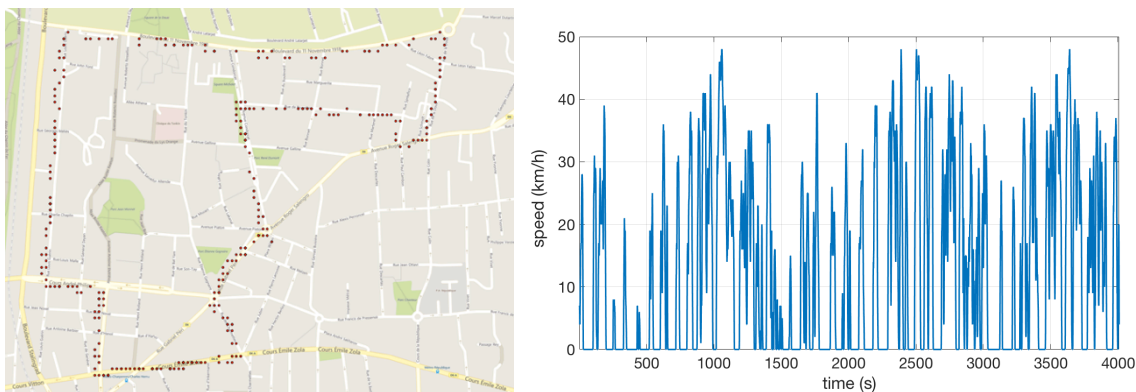


270  
 271

Figure 2 Convexity property of fuel consumption function for Passenger Cars

272 **Measured driving cycle**

273 We now illustrate these effects based on real data. The equipped vehicle was driven in an urban  
 274 area in the eastern part of Lyon (Fig. 3 - left). The speed profile was recorded using GPS for over  
 275 an hour (Fig. 3 - right).  
 276



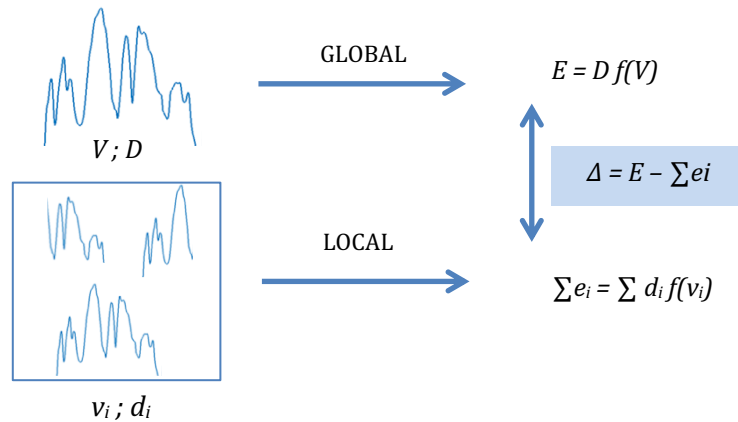
277  
 278

Figure 3: Left: route of the equipped vehicle in the Tonkin district of Lyon.  
 Right: Speed profile measured with GPS for 4000s.

279 Fuel consumption and NOx emissions associated with the whole trip are evaluated using COPERT  
 280 emission functions. This assessment relies on **global** traffic variables ( $V$ ;  $D$ ). On the other hand,  
 281 the driving cycle was split into sub-trips. The proposed decomposition leads to the definition of  
 282 sub-cycles lasting several minutes. For each sub-cycle, the emission assessment relies on **local**  
 283 traffic variables ( $v_i$ ;  $d_i$ ). The sum of these local emissions is compared to the global emission. As  
 284 discussed previously, in order to assess the global emission, we can use the proper mean spatial  
 285 speed, i.e. the time-weighted average of sub-cycle speeds ( $V_t$ ) or the distance-weighted average  
 286 ( $V_d$ ), which is meant to limit the interscale gap. The global distance  $D$  is simply the sum of the  
 287 distances of the sub-cycles ( $d_i$ ).



288 Four decompositions were considered: 15min, 6min, 3min and 1min sub-cycles. Table 1 shows  
 289 for each sub-cycle decomposition, (i) the global mean speeds  $V_t$  and  $V_d$  and (ii) the associated gaps  
 290  $\Delta$  between the global emission and the sum of the local emissions. The discrepancies are expressed  
 291 as a relative deviation from the sum of local emissions.



292 With the distance-weighted mean speed  $V_d$ , the discrepancies between both scales are lower and  
 293 of the opposite sign. In that case, local emissions are higher than the global emission (Fig. 4). This  
 294 plot also exhibits the fact that the time-weighted mean speed  $V_t$  and the associated emission are  
 295 insensitive to temporal partitioning.

296 It finally appears that the shorter the sub-cycle, the larger the gap, which is explained by the  
 297 greater heterogeneity of local speeds. Thus, for FC assessments, the global/local gaps vary  
 298 between -1.1% to -3.3%, while time periods are becoming smaller. For NOx assessments, the  
 299 discrepancies are a little smaller, varying between -0.8% and -1.8%.

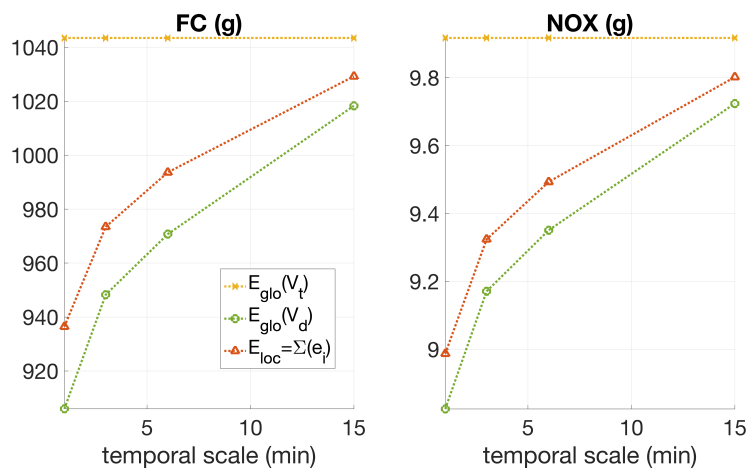


**Figure 4 : Fuel consumption and NOx emissions for various temporal decompositions (from 1 to 15min): sum of the local estimations and global estimations with  $V_t$  and  $V_d$ .**

300  
 301

Driving cycle		$V_t$ (km/h)	$V_d$ (km/h)	$\Delta(V_t)$ (g)		$\Delta(V_d)$ (g)	
15 min	FC	12.51	13.04	14.22	1.4%	-10.94	-1.1%
	NOX			0.12	1.2%	-0.08	-0.8%
6min	FC		15.21	49.8	5.0%	-22.91	-2.3%
	NOX			0.42	4.5%	-0.14	-1.5%
	FC		16.05	70.00	7.2%	-25.19	-2.6%

<b>3min</b>	NOX			0.59	6.4%	-0.15	-1.6%
<b>1min</b>	FC	18.52		107.02	11.4%	-30.50	-3.3%
	NOX			0.93	10.3%	-0.16	-1.8%

**Table 1: Fuel consumption and emission gaps  $\Delta$  for various temporal partitions (from 1 to 15min) and two different global mean speed definitions (distance- or time-weighted).**

302  
303

304 Here, the differences of emissions were highlighted for a driving cycle. By adopting the same  
305 method in the next paragraph, these gaps are evaluated at the level of a vehicle flow passing  
306 through a network.  
307

### 3.2. From cycles to traffic flow

308  
309

310 The construction of the COPERT calculation scale comprises a vehicle and driving cycle lasting  
311 several minutes. In practice, the model is applied more extensively to traffic flow (i.e. various  
312 vehicle technologies and driving cycles), especially for emission inventories. In terms of  
313 kinematics, the average flow speed is then used as an indicator of the amount of emission emitted  
314 per km. The total emissions are calculated as the product of the total travel distance and the  
315 unitary emission factors.

316 In terms of fleet composition, unitary emission factors for each vehicle class are defined as a  
317 weighted average of vehicle technology unitary emission functions. Here, we will focus on  
318 passenger cars. The fleet composition chosen is the French urban fleet for the year 2015 obtained  
319 from the IFSTTAR fleet updated in 2013. This passenger car fleet is composed of 30% EURO 5  
320 diesel vehicles and 24% EURO 4 diesel vehicles.

321 Knowing that the emission curves associated with each vehicle technology hide a wide range of  
322 measured emissions, this large scale is often considered more valid because it is meant to reduce  
323 the uncertainty on emissions. In this article, whatever the scale, an average vehicle is considered  
324 in the sense that the fleet composition is assumed to be homogeneous. On the other hand, dynamic  
325 traffic simulation is used to estimate the traffic variables needed to calculate emissions at all scales  
326 in an accurate and consistent way.  
327

328 Considering an urban network, the total emission  $E_{global}^k$  for pollutant  $k$  related to the traffic flow,  
329 can be assessed as follows:

$$E_{global}^k = D f^k(V_t)$$

331 where

332  $f^k$  is the COPERT unitary emission factor (g/km) of pollutant  $k$ ,  $D$  the total travel distance (km)  
333 and  $V_t$  the mean travel speed (spatial mean speed, see section 2.1).  
334

335 From more detailed traffic data it is possible to determine local emissions. The simplest and most  
336 natural way to partition a network is by road sections. Emissions are then determined for each  
337 link from the local traffic variables:  $d_i$  and  $v_i$ . The total emissions are then evaluated by summing  
338 the estimated emissions on each link  $E_{local}^k = \sum_i d_i f^k(v_i)$ .  
339

340 Thus, the gap in emissions between a calculation at the network scale (global) and a calculation  
341 with spatial decompositions (local) can be formulated as follows, by including the mean speed  $V_d$ :

$$\begin{aligned} \Delta &= E_{global} - E_{local} = D \cdot (f(V_t) - \frac{\sum d_i f(v_i)}{D}) \\ &= D \cdot (f(V_t) - f(V_d)) + D \cdot (f(V_d) - \frac{\sum d_i f(v_i)}{D}) \end{aligned} \quad (4)$$

346  
347

348 The bias  $\Delta$  is proportional to the total travel distance  $D$  and can be seen as a combination of two  
349 terms:

- 350 i. The first term quantifying the impact of the mean speed definition. This term is positive,  
 351 because  $V_d$  is greater than  $V_t$  and  $f$  is decreasing at low speeds.  
 352 ii. The second term quantifying the convexity of the emission functions is negative.

353

354 Using a distance-weighted average speed  $V_d$  as an indicator of the mean flow speed, the first term  
 355 is null. This speed definition is not the right speed definition, but it cancels the first term, which  
 356 certainly has a positive impact on the result.

357

358 Moreover, if we assume that function  $f$  can be approximated by a polynomial of order three, the  
 359 emission gap can then be approached as follows:

360

$$\begin{aligned}
 362 \Delta(V_d) &\approx \Delta^* \\
 361 &= a_2 D \left( V_d^2 - \sum_i \frac{d_i v_i^2}{D} \right) + a_3 D \left( V_d^3 - \sum_i \frac{d_i v_i^3}{D} \right) \\
 363 &= D [(-a_2 - 3\mu a_3)\mu_2 - a_3\mu_3] \qquad (5)
 \end{aligned}$$

364

365

366 With the  $V_d$  centered moments:

$$\mu = V_d$$

$$\mu_2 = \sigma_d^2 = \frac{1}{\sum d_i} \sum d_i (v_i - V_d)^2$$

$$\mu_3 = \frac{1}{\sum d_i} \sum d_i (v_i - V_d)^3$$

367

368 This scaling bias therefore characterizes the heterogeneity of local variables with respect to the  
 369 global scale. In this paper, we discuss two implementations of these scale transformations: (i)  
 370 from local to global and (ii) from global to local. In each case, the same theoretical background as  
 371 described above is involved.

372 Case (i) is discussed in section 4. We assume that we have access to all local traffic data thanks to  
 373 microsimulation. When an emission calculation is needed at larger scale (e.g. area, city), there  
 374 might be a temptation to aggregate traffic data to calculate global emissions (e.g. inventory  
 375 compilation). The scaling bias introduced when performing a single emission calculation at higher  
 376 scale is shown. Then, a methodology for consistent global emissions assessment is proposed.

377 Case (ii) is addressed in section 5. This direction is more challenging. We assume that we have a  
 378 correct information on traffic variables at large scale, on which we intend to conduct an emission  
 379 calculation. This scale is not consistent with the reference scale. Indeed, the reference scale is  
 380 unknown but we believe it is rather local. Thus, the results at large scale will be affected by a  
 381 scaling bias. The objective is to estimate the total emission that correspond to the integration of  
 382 local (close to the reference) emissions. But we do not have access to all local data. This is  
 383 especially the case when using innovative data as floating car data. These partial traffic data are  
 384 quite efficient for deriving mean speed accurately, but they make the estimation of travel distance  
 385 challenging. We are therefore faced with two issues: non scalability and total distance estimation.

386

## 387 4. Results

388

389 In the context of urban scale inventories and monitoring, it is relevant to perform a single emission  
 390 calculation for a whole network. This global scale is sometimes also chosen by default, i.e.  
 391 according to the traffic data available. However, if traffic information is available locally, it may be  
 392 interesting to make several emission calculations locally, to obtain the emission distribution over  
 393 the network.

394

395 In the following sections, the traffic simulation under study is described, as are the space-time  
396 decompositions used to calculate emissions. Finally, the biases between scales are assessed and  
397 analyzed.  
398

#### 399 4.1. Traffic simulation

400  
401 The network presented in Figure 4 is in the 6<sup>th</sup> district of Paris. It is composed of 234 links, 93  
402 crossroads, 19 entries, 21 exits, 4 parking areas and 27 traffic lights. The traffic microsimulation  
403 was implemented on the Symuvia platform<sup>1</sup>, which gives access to the position, speed and  
404 acceleration of each vehicle on the network with a 1s-resolution. Vehicle routing choices were  
405 governed by a dynamic traffic assignment model, which guided each vehicle in the network on the  
406 route that minimized its travel time to its initially assigned destination. Vehicle movements at the  
407 microscopic scale were governed by a set of rules, including car-following modelling (Leclercq,  
408 2007a, 2007b), lane-changes (Laval and Leclercq, 2008) and specific movements at intersections  
409 (Chevallier and Leclercq, 2007). The question of using the platform outputs for pollutant emission  
410 estimations was addressed in (Vieira da Rocha et al., 2013).  
411

412 The simulation consists of 3 hours representing the morning rush hour. The Origin-Destination  
413 matrix was calibrated with hourly traffic flow rates measured on typical weekdays. The total  
414 demand evolved by 15-minute steps (Fig.5).

415 The traffic outputs are the vehicle trajectories, which were aggregated into traffic variables (mean  
416 speeds and travel distances) to correspond to the required COPERT inputs, according to the  
417 observation scale considered.  
418  
419

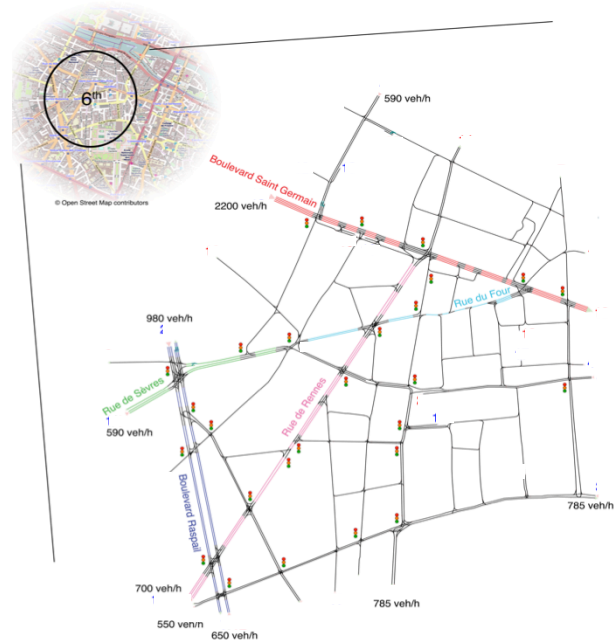
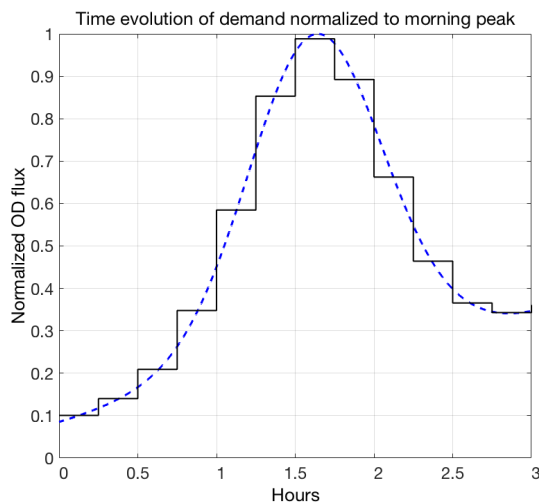


**Figure 5: Traffic microsimulation of the 6<sup>th</sup> district of Paris: evolution over time of normalized input flow (left) and the main peak input flows (right)**

#### 420 4.2. Defining the observation scale

421

<sup>1</sup> <http://www.licit-lyon.eu/themes/realisations/plateformes/symuvia/>

422 The purpose of this study is to evaluate emissions obtained from a dynamic traffic simulation by  
423 performing COPERT calculations for different spatial decompositions. Detailed traffic data are  
424 available (i.e. 1Hz vehicle trajectories) and can be aggregated spatially and temporally. This  
425 section highlights how vehicle trajectories are split and how traffic data are then combined before  
426 computing the emissions.

427  
428 Regarding the traffic microsimulation, the decision was made to set 6-minute time periods  
429 throughout the study. This temporal dynamic allows observing the occurrence of congestion and  
430 its evolution. A description of this phenomenon is required to accurately assess traffic-related  
431 emissions. It is also typical of traffic measurements.

432 On the one hand, the emissions were determined at the global scale (i.e. one calculation for the  
433 whole network). On the other hand, two local spatial decompositions were defined: (i) individual  
434 road sections  $SD_A$ , (ii) individual vehicles  $SD_B$ . These are related to the two types of traffic  
435 measurements: stationary measurements (electromagnetic loops) and mobile ones (probe  
436 vehicles). In each case, the sum of local emissions is compared with global emissions (all links or  
437 vehicles combined) in a more or less congested situation, without favoring one scale over the  
438 other.

439  
440 The *vehicle decomposition*  $SD_B$  is close to the scale at which the chassis dynamometer  
441 measurements were taken. In this case, the driving cycles are 6 min long at most but can also be  
442 shorter because they depend on the time the vehicle entered the network and the time period  
443 considered. This coupling does not aim to provide an estimate of the emission associated with a  
444 specific vehicle but to describe the emission of an average vehicle (respecting the average  
445 specifications associated with the fleet under consideration) presenting such a speed profile.

446  
447 The *road section decomposition*  $SD_A$  is based on a driving cycle per link, combining the trajectories  
448 of the vehicles located on this link for a given 6min time period. These speed profile features  
449 (mean travel speed and travel distance) are used to determine the associated emissions.

450  
451 Similarly, the overall calculation is equivalent to establishing a driving cycle based on the speed  
452 profiles of all the vehicles on the network for a given period, which can be used to evaluate  
453 emissions. Thus, for each emission calculation resolution investigated, the cycle characterizing  
454 the traffic conditions must be constructed by splitting and/or combining the individual  
455 trajectories.

456

### 457 **4.3. Interscale bias for both spatial decompositions**

458

459 This section presents the results in terms of traffic and emissions for the different scales.

#### 460 **4.3.1. Traffic variables**

461

462 For each spatial decomposition, the global network traffic variables required to calculate global  
463 emissions (mean travel speeds and total travel distance) were determined over the thirty 6-min  
464 time periods. As discussed in section 2, the mean travel speed is not transferable from one spatial  
465 partitioning to another. In order to observe scale consistency, the right definition of global mean  
466 travel speed appears to be the time-weighted average of local mean speeds.  $V_t =$   
467  $\sum d_i / \sum \tau_i = \sum (\tau_i v_i) / \sum \tau_i$ , where  $d_i$  and  $\tau_i$  are the cumulative travel distance and travel time  
468 variables associated with the  $i^{\text{th}}$  element (a link or a vehicle) and  $v_i$ , the corresponding mean travel  
469 speed. The distance-weighted average speed  $V_d$  will also be evaluated, because it is assumed to  
470 reduce the emission gaps between the global and local calculation scales, see section 3.1.

471

472 The temporal evolution of these global traffic variables is shown in Figure 6. We observe that the  
473 time-weighted speed is lower than the distance-weighted speed, especially when subject to

474 congestion (around period 19). Indeed, this speed definition captures the traffic dynamics  
 475 correctly. On the other hand, Figure 5 shows that the distance-weighted speed depends on the  
 476 local scale: the global speed evaluated from the links ( $SD_A$ ) is higher. This is explained by the  
 477 Wardrop relationship (formula (2)) and the fact that local speed variance between individual  
 478 vehicles is smaller than the speed variance between individual road sections. Thus, during  
 479 congestion the average network speed varies between 7.5 and 16.6 km/h, depending on the speed  
 480 definition.

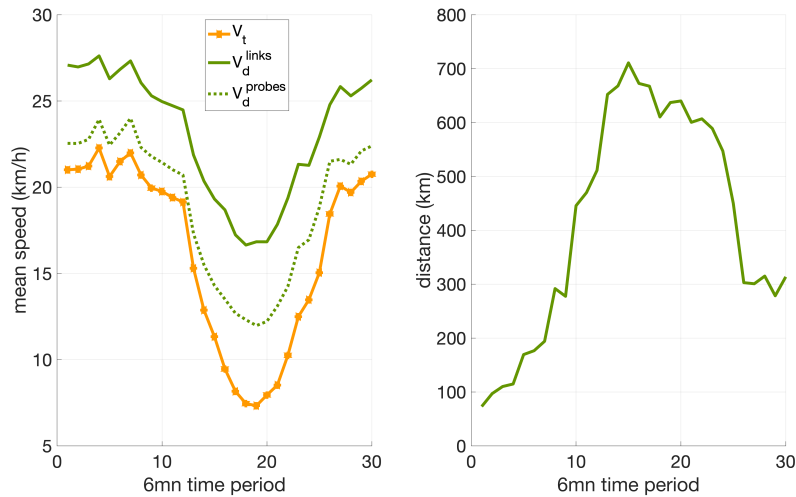


**Figure 6: Time evolution of global traffic variables (left: global mean speeds; right: total travel distance)**

481  
 482 Figure 7 illustrates the distribution of both traffic variables over both spatial decompositions. The  
 483 results are presented for a congested time period, for which the discrepancies are obviously more  
 484 significant. Regarding speeds, the wide dispersion of values on the road section decomposition  
 485  $SD_A$  is highlighted, which leads to a higher global mean speed  $V_d$  (16.8km/h versus 7.9km/h for  
 486  $V_t$ ). For vehicle decomposition  $SD_B$ , the speeds are less heterogeneous, which leads to a lower  
 487 global mean speed  $V_d$  (12.2 km/h). As far as the total travel distance is concerned, it is on average  
 488 2.7 km for the road sections ( $SD_A$ ), versus 0.41 km for the vehicles ( $SD_B$ ).  
 489

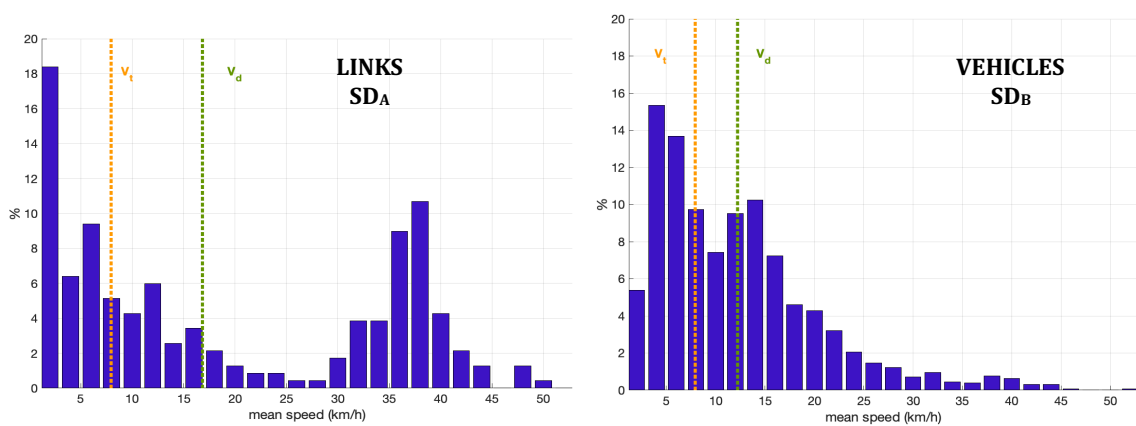


**Figure 7: Distributions of local mean speeds subject to congestion for both spatial decompositions (left:  $SD_A$ ; right:  $SD_B$ ).**

505

#### 506 4.3.2. Fuel consumption and NOx emissions

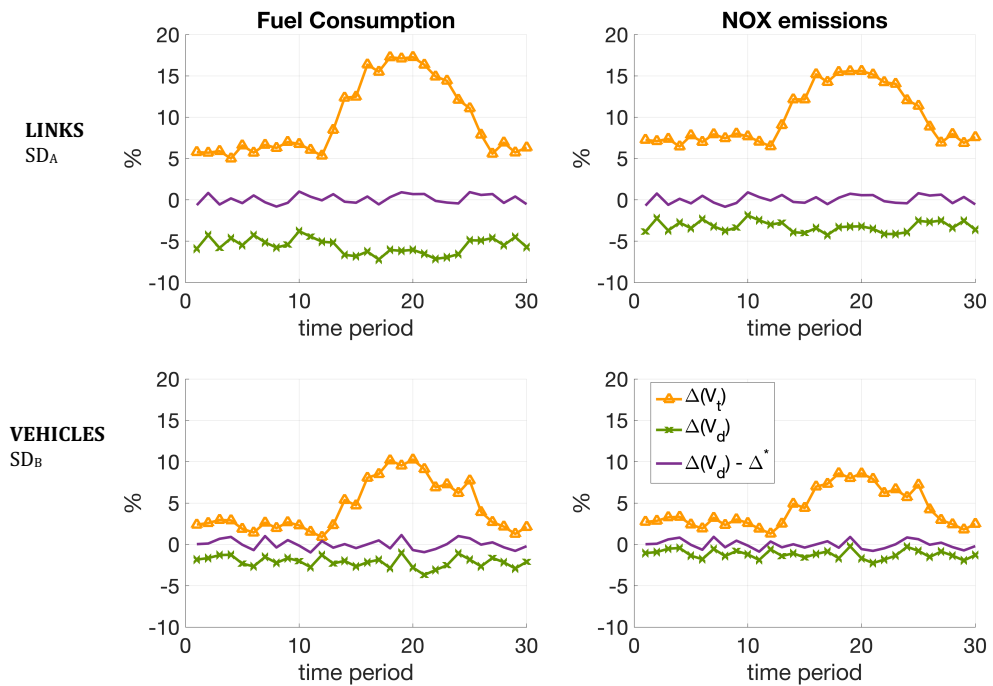
507

508 Regarding the environmental assessments, fuel consumption and NOx emissions are evaluated  
 509 and presented in each case. The local traffic variables described in the previous section were used  
 510 (i) to assess the associated local emissions, (ii) to evaluate the global traffic variables needed to  
 511 assess the global emissions, and (iii) to estimate the interscale bias  $\Delta^*$  using formula (5).  
 512 Both global mean speed definitions were tested. The corresponding global emissions  $E(V_t)$  and  
 513  $E(V_d)$  were evaluated, such as the gaps  $\Delta(V_t)$  and  $\Delta(V_d)$ . The discrepancies are expressed as a  
 514 relative deviation from the sum of local emissions.  
 515 Table 2 summarizes the results for a congested 6min time period. After removing  $\Delta^*$ , i.e. the  
 516 interscale bias estimated from  $\mu, \mu_2, \mu_3$ , the relative gaps are lower than 1%.  
 517  
 518

		$V_t$ (km/h)	$V_d$ (km/h)	$\mu_2(V_d)$	$\mu_3(V_d)$	$\Delta(V_t)$	$\Delta(V_d)$	$\Delta(V_d) - \Delta^*$
SD <sub>A</sub>	FC	7.3	16.8	174.0	1445.9	17.1%	-6.2%	0.9%
	NOX					15.6%	-3.2%	0.7%
SD <sub>B</sub>	FC	7.3	11.9	51.2	450.6	9.5%	-1.0%	1.1%
	NOX					8.0%	-0.2%	0.9%

519 **Table 2 Comparison of global mean speeds, aggregated from both spatial decomposition (SD<sub>A</sub> and SD<sub>B</sub>) for a**  
 520 **congested time period. When estimating FC and NOx at both local and global scales, the scaling bias  $\Delta$  is**  
 521 **alleviated by using  $V_d$  instead of  $V_t$ , and is almost cancelled by using the extensive formulation  $\Delta^*$**

522 This means that by integrating the effect of spatial decomposition on emissions in traffic data  
 523 processing, it is possible to significantly reduce the differences between emission calculation  
 524 scales. To do this, it is necessary to use the definition of the average speed weighted by distances  
 525 and to evaluate the interscale bias  $\Delta^*$ . For spatial decomposition SD<sub>A</sub>, the gap is reduced from 17%  
 526 for FC (16% for NOx) to less than 1% and for SD<sub>B</sub>, from 11% for FC (5% for NOx) to less than 0.1%.  
 527 Figure 8 shows the temporal evolution of these deviations for the two spatial partitions  
 528 considered (SD<sub>A</sub> and SD<sub>B</sub>).  
 529



540  
541  
542 **Figure 8 Relative gaps of consumptions and emissions**  
 543 **with the links (top) and probes (bottom) approach.**  
544  
545  
546  
547  
548  
549  
550  
551  
552

553  
554  
555  
556  
557  
558  
559  
560  
561  
562  
563  
564  
565  
566  
567  
568  
569  
570  
571

It can be seen that with  $V_t$ , the gaps are particularly visible in congestion and can reach 10% and more. On the other hand, with  $V_d$  the gaps are reduced and have opposite signs. They are also more or less constant regardless the traffic conditions. Finally, after removing the estimated bias, the gaps between the scales are almost null (under 1%) whatever the traffic conditions.

Thus, based on a global emission calculation and knowledge of the heterogeneity of speeds on the local elements, it is possible to retrieve the emissions evaluated using a local approach and thereby ensure consistent results between scales. To alleviate the scaling bias, we can simply use the distance-weighted average of local speeds. An extensive formulation of the scaling bias is also proposed to restore consistency.

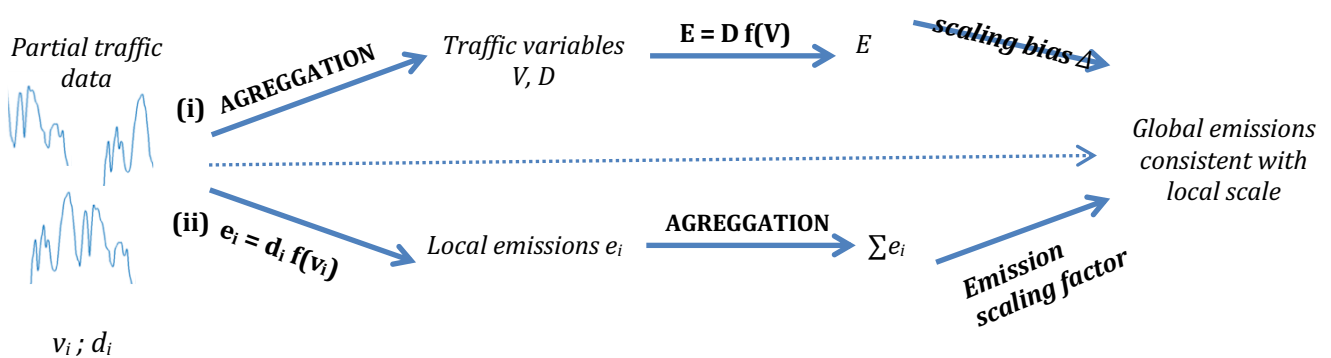
Lastly, final objective is to ensure that emissions are consistent with the COPERT reference scale. As noted in section 2.2, we do not have exact knowledge of the reference scale for the COPERT laws and thus require access to traffic information at that scale. In the following section, we place ourselves in this particular case, knowing that we have partial local traffic data. The reference scale is unknown, but we believe it is rather local. We assume that 6min probe data (corresponding to driving cycles of an average length of 400m) represent our reference scale.

### 5. Practical application: estimating global emission from a sample of probe vehicles

572  
573  
574  
575  
576  
577  
578  
579  
580  
581  
582  
583

After having highlighted the scaling bias associated with the calculation of emissions and proposed a method for reducing this bias based on a traffic simulation, we now focus on applying the method to a real situation. In this case, our objective is to characterize the emissions associated with a network (neighborhood, city area, etc.) using a new data source, namely a sample of vehicle trajectories. This type of data is becoming increasingly available thanks to tracking devices in vehicles (in particular GPS).

We then have two options: (i) that of determining the global traffic variables and the associated emissions, or (ii) that of determining the local emissions (i.e. of each vehicle) and add them together.



584  
585  
586  
587  
588  
589  
590  
591  
592  
593  
594

In case (i), we make an error on network emission due to the introduction of a scaling bias. In case (ii), the scale is in better accordance with the reference scale. However, we do not have access to all vehicle data, so we need to shift from the emissions of partial observations to the full population emissions. Determining this emission scaling factor is very challenging and will certainly introduce large uncertainties. That is why this alternative is not the most reliable and thus not considered here. Finally, option (i) is selected: the emissions are estimated on a global scale, and then corrected using the scaling bias estimates. In this way, the corrected global emissions are rather close to local emissions.

In addition to this scale inconsistency issue, we are faced with the issue of accurate assessment of global traffic variables needed for calculating emissions from probe samples. Here, we draw a



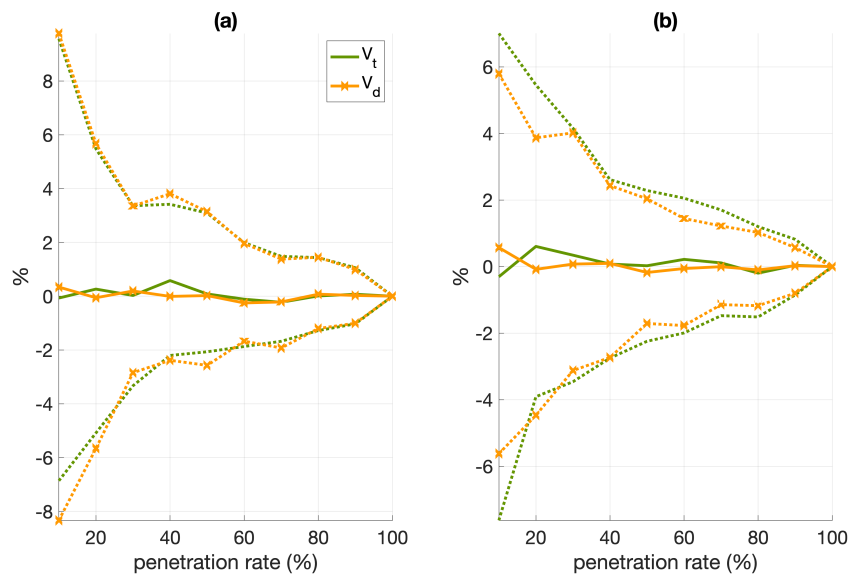
595 random sample of vehicles from the simulation to represent floating car data. We can therefore  
 596 test various penetration rates of the probe vehicles (i.e., the ratio between the number of probes  
 597 and the total number of vehicles on the network) and evaluate the quality of the estimates.  
 598

### 599 5.1. Mean speed estimation

600  
 601 (Leclercq et al., 2014) compared the methods to estimate the overall mean speed  $V_t$  from loops or  
 602 probe samples. This study showed that an optimal probe sampling rate of 20% allows efficiently  
 603 capturing the mean spatial speed, with an error of less than 10%. But as mentioned above, it is  
 604 more appropriate to evaluate emissions from an estimate of the distance-weighted speed  $V_d$  in  
 605 order to reduce the scaling bias. We propose here to evaluate the relevance of new statistical  
 606 indicators, weighted by distances.  
 607

608 The penetration rate  $\tau$  (i.e., the ratio between the number of probes and the total number of  
 609 vehicles on the network) will be considered constant over time. This is a simplification, as in  
 610 reality the data collected do not represent a constant penetration rate. The effect of variable  
 611 penetration rate has been discussed in (Lejri et al., 2014). For each period and penetration rate,  
 612 100 probe samples are drawn randomly in the traffic microsimulation and the estimators of the  
 613 variables of interest are assessed for each sample. Their quality is evaluated in comparison to the  
 614 variable of the total population (all vehicles).  
 615

616 The variability of the results obtained for 100 probe samples is represented in the following  
 617 figures by the median value (solid line) and the 1<sup>st</sup> and 9<sup>th</sup> deciles (dotted lines). Thus, 80% of the  
 618 data is between the dotted lines. The variables are all expressed as a relative error to the variable  
 619 of the total population:  $(\bar{x} - x)/x \times 100$ .  
 620



621  
 622 **Figure 9 Relative errors on mean speeds  $V_t$  and  $V_d$  depending on the penetration rate**  
 623 **in (a) free flow conditions and (b) congested conditions**

624 Figure 9 confirms previous works: mean speeds may be assessed from probes with good accuracy,  
 625 whatever the traffic conditions. Thus, with a penetration rate of 20%, we can estimate  $V_d$  with an  
 626 error of less than +/- 5.7% for 80% of the samples in free flow and between -4.5% and +3.8% in  
 627 congestion.  
 628

629 **5.2. Total travel distance estimation**

630

631 The second variable to be assessed is the total travel distance. The distance travelled by a sample  
632 of vehicles is available, but we must determine a scaling factor to obtain the distance travelled by  
633 all the vehicles during the time period. In contrast to mean speed estimation, this issue is quite  
634 challenging. In the first approximation, this distance scaling factor can be derived from the  
635 penetration rate  $\tau$ , which is reached during the random draw. The total travel distance  $D$  is then  
636 assessed by  $d_{probes}/\tau$ , assuming that the number ratio is relevant for estimating the distance  
637 ratio.

638

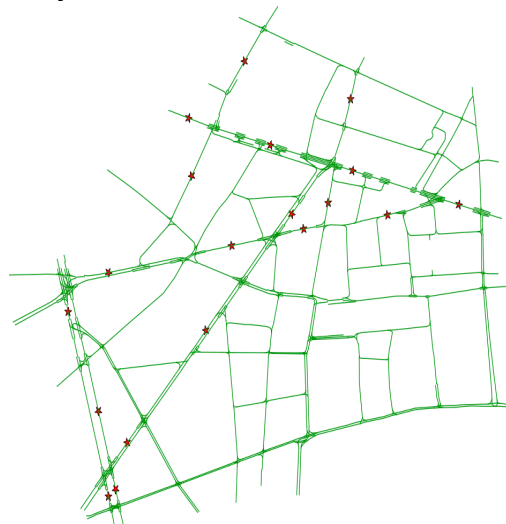
639 But in a real case, this rate is variable over time and above all unknown. That is why it will also be  
640 estimated by the “probe fishing” method first proposed in (Geroliminis & al., 2008). In addition  
641 to the probes, this method requires a minimal number of loop detectors that permit measuring  
642 the flows. The penetration rate is then estimated as the ratio of probes crossing the loops over the  
643 total observed flow, see eq. (6).

644 
$$\tau^*(T) = \frac{\sum_k N_{probes}^k(T)}{\sum_k N_{vehicles}^k(T)} \quad (6)$$

645 where  $N_{probes}^k(T)$  is the number of probes seen on loop  $k$ , during time period  $T$  and  $N_{vehicles}^k$  the  
646 number of vehicles seen on loop  $k$ , during time period  $T$ .

647

648 Note that the loop requirement is not an issue in practice as loop data are usually available in  
649 urban areas, at least in minimal quantity. We identified around twenty detector loops on the real  
650 network (Fig. 10), which represents about 10% of the links. For each time period, using  
651 microsimulation, we are able to identify the route of the probe vehicles and therefore the loops  
652 they cross. We can then estimate the ratio between the number of probe vehicles and the total  
653 number of vehicles seen on the loops during a given period. With on-field data, it is also very easy  
654 to know which loop is crossed by vehicles based on their GPS coordinates.



655

656

657

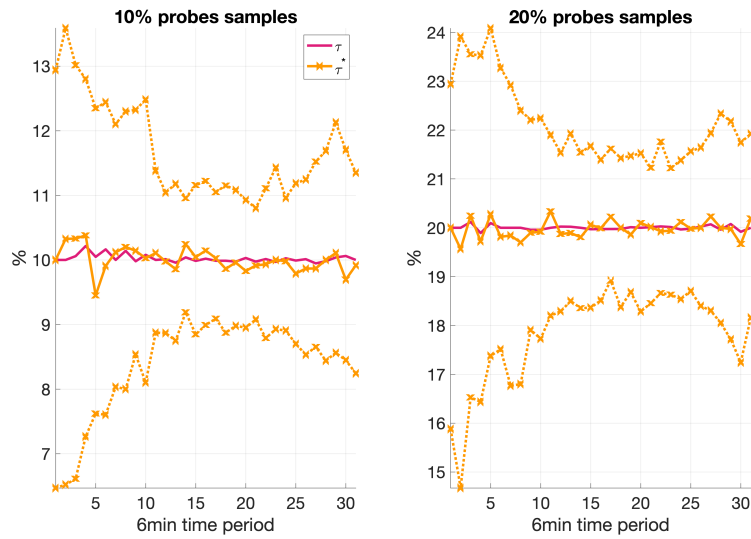
**Figure 10 Location of major loops in the sixth district of Paris<sup>2</sup>**

658

659 Then, the distance scaling factor will be used and its impact on reducing scaling bias will be  
660 assessed. Using the fishing method, the penetration rate  $\tau$  is estimated quite precisely during  
661 congestion, whereas in free flow the errors range from 7% to 13% for a 10% sample and from  
662 15% to 24% for a 20% sample (Fig. 11). This is simply because fewer vehicles are traveling in the  
663 network in free-flow, rendering the estimate less robust.

---

<sup>2</sup> <https://opendata.paris.fr/explore/?sort=modified&q=trafic> (accessed 2019/09/06)

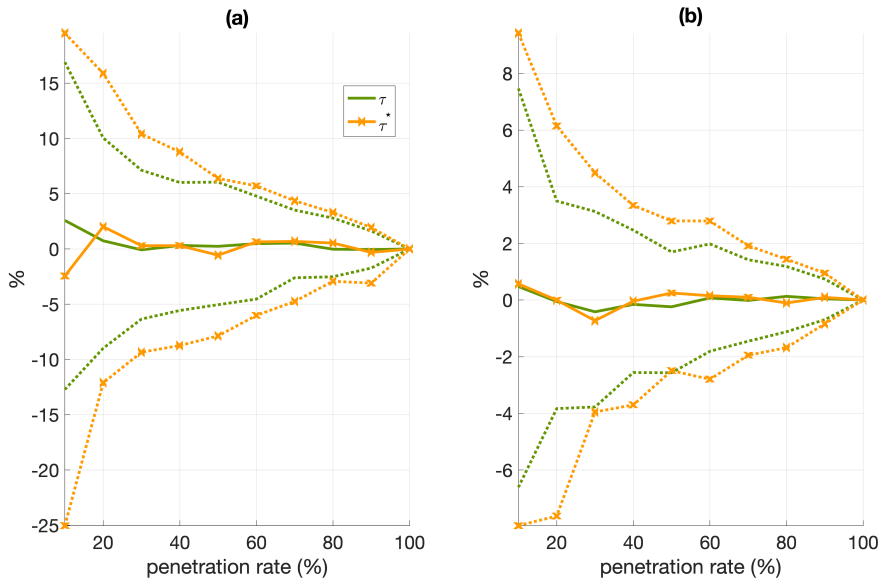


665  
666

Figure 11 Time evolution of penetration rates:  $\tau$  and the estimate  $\tau^*$  (fishing).

667

668 The penetration rate is then used to infer the total travel distance, which is a critical parameter  
 669 for estimating emissions. Figure 12 highlights the relative errors on total travel distance assessed  
 670 from the sample travel distance and the vehicle number ratio (penetration rates  $\tau$  and  $\tau^*$ ).  
 671 Obviously, these estimates are better when the penetration rate increases. We can first observe a  
 672 break for a penetration rate of 20%, beyond which the relative errors decrease significantly. Using  
 673 the fishing method and 20% probe samples, it is possible to assess the total travel distance with  
 674 an error of +/-15% in free flow and +/-6% in congestion.  
 675



676  
677  
678

Figure 12 Relative errors on total travel distance with a known penetration rate  $\tau$  and an estimated penetration rate  $\tau^*$  in (a) free flow conditions and (b) congested conditions

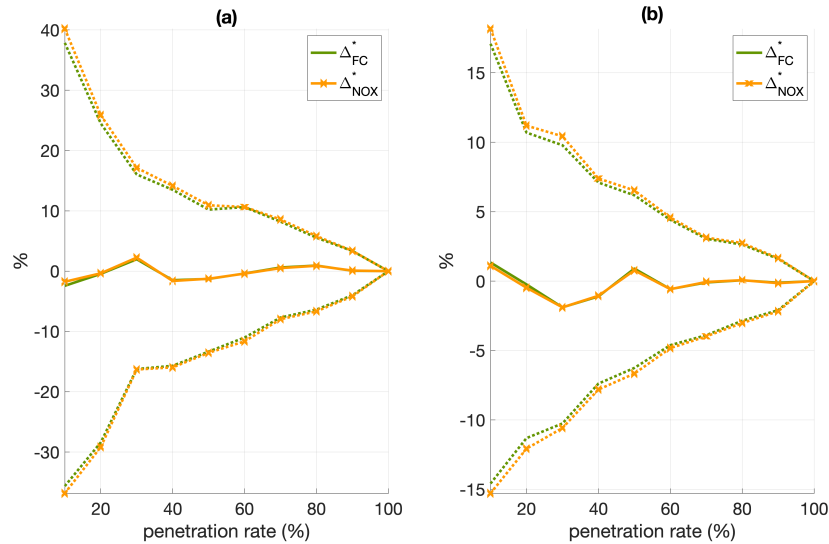
679

680 **5.3. Scaling bias estimation**

681

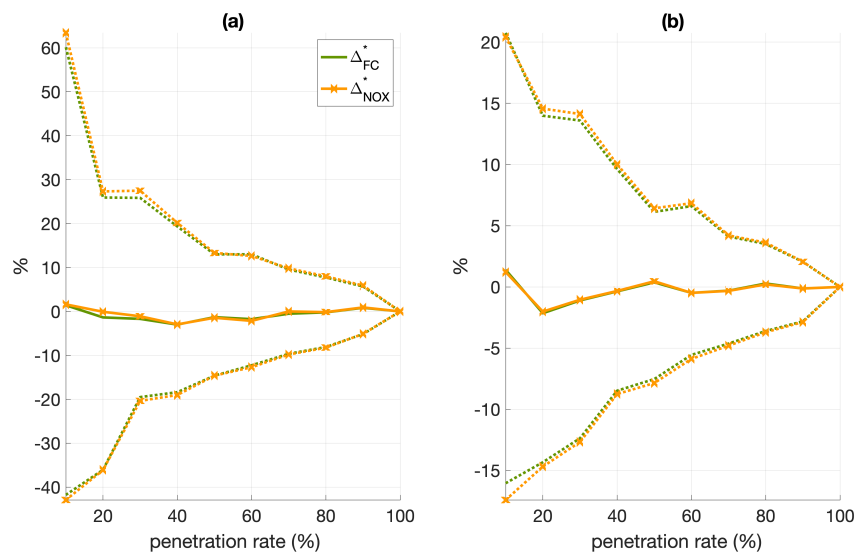
682 Once the global traffic variables have been assessed, it is possible to evaluate the global emissions.  
 683 This estimate will be subject to the scaling bias described in section 3.2. The next step is therefore

684 to evaluate the bias to be removed in order to better estimate the results corresponding to the  
 685 integration of local emissions, which, here, are assumed to be close to the reference scale. The  
 686 variables  $V_d$ ,  $\mu_2$  and  $\mu_3$  and  $D$  are first estimated from the probe samples. We then evaluate the  
 687 scaling bias  $\Delta^*$  using formula (5). In order to distinguish the influence of sampling on the speed  
 688 and travel distance assessment, the total travel distance per time period is first assumed known.  
 689 Figure 13 presents the relative errors on the scaling bias  $\Delta^*$ . In free flow, with 20% probe samples,  
 690 the errors are in the range of -29% to 26% and -12% to 11% in congestion. These errors are  
 691 significant and equivalent for fuel consumption and NOx emissions.



692  
 693 **Figure 13 Relative errors on scaling bias  $\Delta^*$  depending on the penetration rate**  
 694 **in (a) free flow conditions and (b) congested conditions, assuming the total travel distance is known.**

695 When total travel distance is estimated by the fishing method (Fig. 14), the gaps increase even  
 696 further, in the range of -37% to 26% and +/-15% in congestion. We note that the outcomes are  
 697 worse than for speed estimation. A 40% sample is required to estimate the bias with an accuracy  
 698 of about 10%.

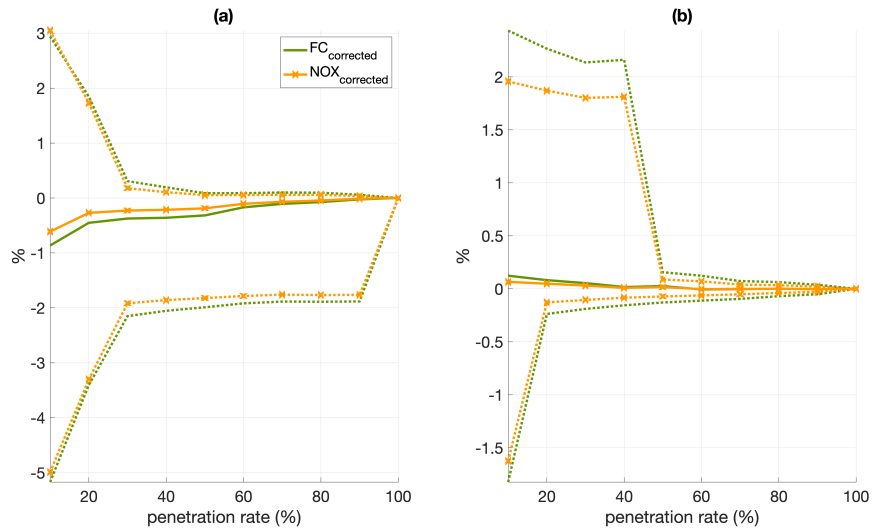


699  
 700 **Figure 14 Relative errors on scaling bias  $\Delta^*$  depending on the penetration rate**  
 701 **in (a) free flow conditions and (b) congested conditions, assuming the total travel distance**  
 702 **is assessed using the fishing method.**

703

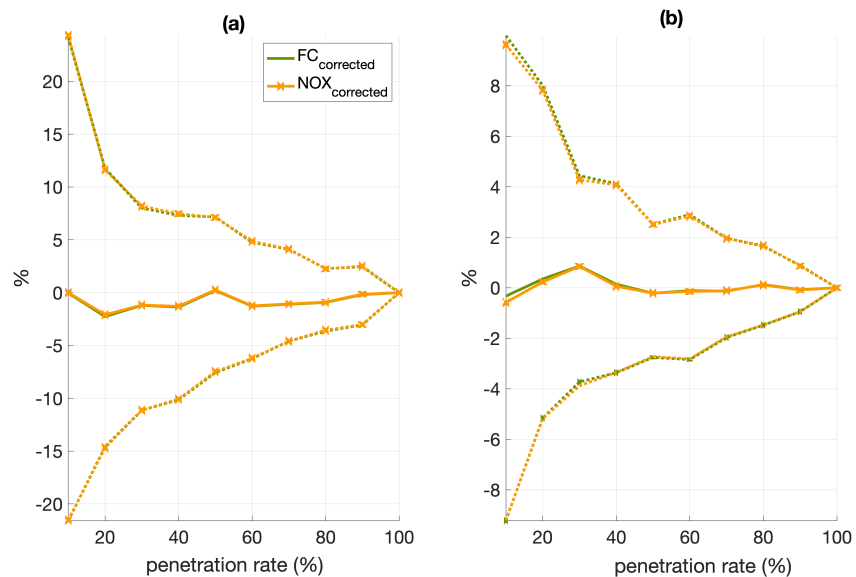
704 **5.4. Corrected emission estimation**

705  
 706 Finally, the global emissions are corrected by removing the scaling bias ( $E(V_d) - \Delta^*$ ) and  
 707 compared to the sum of local emissions. These results are first analyzed as a function of the  
 708 penetration rate. The estimation of corrected emissions is quite accurate when total travel  
 709 distance is assumed to be known (Fig. 15). Indeed, the errors here decrease sharply to the range  
 710 of -3% to 2% in free flow and even less in congestion. This can be explained by the fact that the  
 711 imprecise estimation of  $V_d$  induces errors both on global emissions  $E(V_d)$  and on the error on bias  
 712  $\Delta^*$ , that counterbalance each other.



713  
 714 **Figure 15** Relative errors on corrected emissions  $E(V_a) - \Delta$  depending on the  
 715 penetration rate in (a) free flow conditions and (b) congested conditions,  
 716 assuming the total travel distance is known.

717 Consequently, when total travel distance is assessed by fishing, the relative errors are of the same  
 718 order as those made on total travel distance (Fig. 16). Again, they are almost similar for both fuel  
 719 consumption and NOx emissions. These results confirm that the challenging issue is definitively  
 720 the estimation of total travel distance. The fishing method makes it possible to have a relative  
 721 error on the residual gap within the range of 10% with 20% probe samples in loaded traffic  
 722 conditions.



723  
 724 **Figure 16** Relative errors on corrected emissions  $E(V_a) - \Delta^*$  depending on the  
 725 penetration rate in (a) free flow conditions and (b) congested conditions,  
 726 assuming the total travel distance is assessed using the fishing method.

727 Finally, residual errors are on average very low, even when the distance is approximated: errors  
728 are less than 4% on average for 10% probe samples and less than 2% for 20% probe samples.  
729 This study shows that in a real case, the ability to reduce bias depends on our ability to accurately  
730 estimate total travel distance.

731  
732

## 733 **6. Conclusion**

734

735 To the question “Are average speed emission functions scale-free”, the answer is clearly no.  
736 Basically, the scaling issues occur (i) because of the convexity of the emission law and (ii) because  
737 of the non-scalability of the mean-speed definition. This work pointed out, that the second effect  
738 can be minored if distance-weighted speed definition is used. But this is not the correct definition  
739 of mean speed, which should be distance over time at all scales.

740 More generally, the inconsistency issue is not specific to average speed emission models. We  
741 focused here on COPERT, an average speed model, because its use is very widespread, particularly  
742 at various spatial-temporal scales. However, inconsistency issues occur for any model that either  
743 use non scalable variable, e.g. mean speed, or non-linear emission functions.

744

745 The purpose of this paper was to make emission modelers aware of the scale-inconsistency in  
746 emission calculations and to provide them with a method to restore consistency between the  
747 reference scale (resolution at which the relationship between average speed and emission rates  
748 are established) and the emission calculation scale (spatial decomposition on which emission  
749 factors are implemented). We must specify that the reference scale is not yet properly defined. To  
750 our knowledge, emission laws are developed at local scale (driving cycles) but are not established  
751 for a unique travel length. The reference scale should be related with the scale at which emission  
752 laws are designed, because it is the scale at which mean speed is measured. While we think that  
753 new emission laws should be determined based on a clear definition of a reference scale (see the  
754 discussion), we currently consider that the local scale is the more reliable because it is closer to  
755 the actual driving scale.

756 In this paper, we discuss two implementations of these scale transformations: (i) from local to  
757 global and (ii) from global to local. In each case, the same theoretical background as described  
758 above is involved. In case (i), we focused on two spatial decompositions of a network: individual  
759 road sections and vehicles (local scales). If traffic data are aggregated to calculate emissions on a  
760 larger scale (e. g. district), interscale (local vs global) biases are introduced. This occurs even if  
761 traffic data are properly aggregated (using time-weighted mean speed). From the case study, the  
762 biases range from 5% to 17%, depending on the pollutant, spatial partitioning and traffic  
763 conditions. These discrepancies can be reduced using a distance-weighted mean speed, which is  
764 not a scale-consistent definition of mean travel speed. They can almost be cancelled using the  
765 extensive formulation proposed in this paper, thus consistency can be guaranteed between  
766 emissions assessed at different scales.

767 In case (ii), we assumed that traffic variables can only be estimated at large scale. Thus, we  
768 performed the emission calculations at that global scale. As the emission calculations are not  
769 undertaken at a scale consistent with the reference scale, we then introduced a bias. By reversing  
770 the method presented in this paper, we significantly reduced this scaling bias and obtained better  
771 total emission predictions. This second study is based on probe data. The results are strongly  
772 dependent on the probe sample and the penetration rate, which should be high enough in practice  
773 to properly estimate all the variables. The most critical step is the accurate estimation of total  
774 travel distance. A “fishing” method was applied to this end to improve the estimate of this variable.  
775 We finally managed to reduce the gaps to a maximum of 8% in congestion for a penetration rate  
776 of about 20%.

777

## 778 **7. Discussion**

779

780 Aggregate emission models are commonly used to calculate total emission at different scales  
781 across a country, a region, a city and road sections. The lack of consistency between scales is often  
782 attributed to the lack of completeness and/or accuracy of input data. With regard to traffic data,  
783 it was shown here that accurate and consistent traffic information between emission calculation  
784 scales may lead to different results. This is not satisfactory and we believe that it can be improved.  
785

786 As working with nuclear information like emission per second is not possible in practice, the only  
787 option to alleviate scaling issues, is (i) to properly define the reference scale (where we know that  
788 no error occurs because the model has been designed on this particular scale) and then (ii) to find  
789 numerical transformations that reduce the scaling bias. This is what we tried to do here with the  
790 average speed models despite the absence of a clear reference. This should be the next step and  
791 requires reshaping existing emission laws. We would recommend to this end, to set emission laws  
792 on driving cycles of same distances. Defining the right distance is out of the scope of this study but  
793 the values found in the literature (400 – 500m) seem rather reasonable to us.  
794

795 A review of macroscopic emission models is currently being undertaken in order to develop  
796 emission laws that are more representative of real driving situations (slope, intersections, etc.)  
797 and traffic conditions (free, charged, congested, etc.). Previous works showed the need for  
798 integrating representative real-world driving cycles in the development of emission models  
799 (Fontaras et al., 2017; Franco et al., 2013). Among other issues, the resolution for establishing  
800 emission laws is quite challenging. (Papadopoulos et al., 2018) described how the resolution  
801 affects emission factors. This study also confirms that the extensive use of PEMS data can enhance  
802 the inherent bias of emission functions. Indeed, setting EFs on different lengths means using  
803 multiple and inconsistent average speed values. That is we recommend working with cycles of the  
804 same distance, in order to average observations that are consistent in terms of mean speed  
805 definition. When applying these new emission laws at other scales, we would be able to remove  
806 the scale bias by determining the appropriate corrective factors.  
807

808 Finally, through this study, we mainly focused on emission calculations at large scale. We did not  
809 directly address the issue of calculating emissions at the link level. However, calculating emissions  
810 at this scale attracts more and more attention as it allows (i) obtaining the distribution of local  
811 emissions over the network and (ii) establishing links with traffic model output data and  
812 dispersion models. However, links obviously do not have equal lengths over the network. Then,  
813 even if a clear reference scale is established, using emission laws directly on links would create a  
814 new scale problem. We therefore recommend partitioning the network into virtual links of same  
815 length as the reference scale. Then, emission calculations could be done without scaling bias. The  
816 emissions related to the real links can finally be evaluated in proportion to the distance travelled  
817 in each link. Such a method should be carefully investigated in a future study.  
818  
819

## 820 **Acknowledgments**

821

822 This study has received funding from the European Research Council (ERC) in the framework of  
823 the European Union's Horizon 2020 research and innovation program (grant agreement No  
824 646592 – MAGnUM project).  
825  
826

## 827 **8. References**

828

829 André, M., 2004. The ARTEMIS European driving cycles for measuring car pollutant emissions. *Sci.*  
830 *Total Environ.* 334–335, 73–84. <https://doi.org/10.1016/j.scitotenv.2004.04.070>

831 André, M., Rapone, M., 2009. Analysis and modelling of the pollutant emissions from European  
832 cars regarding the driving characteristics and test cycles. *Atmos. Environ.* 43, 986–995.  
833 <https://doi.org/10.1016/j.atmosenv.2008.03.013>

834 AVL, 2018. Vehicle Driveline Simulation. <https://www.avl.com/cruise>.

835 Barth, M., Barth, M., Malcolm, C., Malcolm, C., Scora, G., Scora, G., 2001. Integrating a  
836 Comprehensive Modal Emissions Model into ATMIS Transportation Modeling Frameworks.  
837 *Transportation (Amst)*.

838 Borge, R., de Miguel, I., de la Paz, D., Lumbreras, J., Pérez, J., Rodríguez, E., 2012. Comparison of  
839 road traffic emission models in Madrid (Spain). *Atmos. Environ.* 62, 461–471.  
840 <https://doi.org/10.1016/j.atmosenv.2012.08.073>

841 Boulter, P.G., McCrae, I.S., 2007. ARTEMIS: Assessment and Reliability of Transport Emission  
842 Models and Inventory Systems – final report. 2007 350.

843 Chevallier, E., Leclercq, L., 2007. A macroscopic theory for unsignalized intersections. *Transp. Res.*  
844 *Part B Methodol.* 41, 1139–1150. <https://doi.org/10.1016/j.trb.2007.05.003>

845 Donato, T., Giovinazzi, M., 2017. Building a cycle for Real Driving Emissions. *Energy Procedia* 126,  
846 891–898. <https://doi.org/10.1016/j.egypro.2017.08.307>

847 Edie, L.C., 1965. Discussion of traffic stream measurements and definitions., in: 2nd International  
848 Symposium on the Theory of Traffic Flow. pp. 8–20.

849 EEA, 2017. Annual European Union Greenhouse Gas Inventory 1990–2015 and Inventory Report  
850 2017. European Environment Agency Technical Report No 6/2017, Copenhagen, Denmark.

851 EMEP/EEA, 2016. Air Pollutant Emission Inventory Guidebook- 2016 28. <https://doi.org/ISSN>  
852 1977-8449

853 Fallah Shorshani, M., André, M., Bonhomme, C., Seigneur, C., 2015. Modelling chain for the effect  
854 of road traffic on air and water quality: Techniques, current status and future prospects.  
855 *Environ. Model. Softw.* 64, 102–123. <https://doi.org/10.1016/j.envsoft.2014.11.020>

856 Fontaras, G., Zacharof, N.G., Ciuffo, B., 2017. Fuel consumption and CO<sub>2</sub> emissions from passenger  
857 cars in Europe – Laboratory versus real-world emissions. *Prog. Energy Combust. Sci.* 60, 97–  
858 131. <https://doi.org/10.1016/j.pecs.2016.12.004>

859 Fontes, T., Pereira, S.R., Fernandes, P., Bandeira, J.M., Coelho, M.C., 2015. How to combine different  
860 microsimulation tools to assess the environmental impacts of road traffic? Lessons and  
861 directions. *Transp. Res. Part D* 34, 293–306. <https://doi.org/10.1016/j.trd.2014.11.012>

862 Franco, V., Kousoulidou, M., Muntean, M., Ntziachristos, L., Hausberger, S., Dilara, P., 2013. Road  
863 vehicle emission factors development: A review. *Atmos. Environ.* 70, 84–97.  
864 <https://doi.org/10.1016/j.atmosenv.2013.01.006>

865 Hausberger, S., Rexeis, M., Zallinger, M., Luz, R., 2009. Emission Factors from the Model PHEM for  
866 the HBEFA Version 3. *Univ. Technol. Graz, Rep. Nr. I-20/2009 Haus-Em* 33, 679.

867 Knoop, V.L., Hoogendoorn, S.P., Van Zuylen, H.J., 2009. Empirical Differences between Time Mean  
868 Speed and Space Mean Speed., in: *Proceedings of Traffic and Granular Flow 07*. pp. 351–356.

869 Laval, J.A., Leclercq, L., 2008. Microscopic modeling of the relaxation phenomenon using a  
870 macroscopic lane-changing model. *Transp. Res. Part B Methodol.* 42, 511–522.  
871 <https://doi.org/10.1016/j.trb.2007.10.004>

872 Leclercq, L., 2007a. Hybrid approaches to the solutions of the “Lighthill-Whitham-Richards”  
873 model. *Transp. Res. Part B Methodol.* 41, 701–709.  
874 <https://doi.org/10.1016/j.trb.2006.11.004>

875 Leclercq, L., 2007b. Bounded acceleration close to fixed and moving bottlenecks. *Transp. Res. Part*  
876 *B Methodol.* 41, 309–319. <https://doi.org/10.1016/j.trb.2006.05.001>

877 Leclercq, L., Chiabaut, N., Trinquier, B., 2014. Macroscopic Fundamental Diagrams: A cross-  
878 comparison of estimation methods. *Transp. Res. Part B Methodol.* 62, 1–12.  
879 <https://doi.org/10.1016/j.trb.2014.01.007>

880 Lejri, D., Can, A., Schiper, N., Leclercq, L., 2018. Accounting for traffic speed dynamics when  
881 calculating COPERT and PHEM pollutant emissions at the urban scale. *Transp. Res. Part D*  
882 *Transp. Environ.* 63, 588–603. <https://doi.org/10.1016/j.trd.2018.06.023>



883 Lejri, D., Ibrahim, N.A., Bécarie, C., Leclercq, L., 2014. Estimating pollutant emissions from  
884 aggregated traffic variables: the influence of data sources and sampling methods, in:  
885 International Symposium of Transport Simulation 2014.

886 Ntziachristos, L., Gkatzoflias, D., Kouridis, C., 2009. COPERT: A European Road Transport Emission  
887 Inventory Model. *Inf. Technol. Environ. Eng.* <https://doi.org/10.1007/978-3-540-88351-7>

888 Papadopoulos, G., Keramydas, C., Ntziachristos, L., Lo, T.-S., Ng, K.-L., Wong, H.-L.A., Wong, C.K.-L.,  
889 2018. Emission Factors for a Taxi Fleet Operating on Liquefied Petroleum Gas (LPG) as a  
890 Function of Speed and Road Slope. *Front. Mech. Eng.* 4, 1–13.  
891 <https://doi.org/10.3389/fmech.2018.00019>

892 Samaras, Christos, Ntziachristos, L., Samaras, Z., 2014. COPERT Micro : a tool to calculate the  
893 vehicle emissions in urban areas. *Transp. Res. Arena 2014* 10.

894 Samaras, C., Tsokolis, D., Toffolo, S., Garcia-Castro, A., Vock, C., Ntziachristos, L., Samaras, Z., 2014.  
895 Limits of applicability of COPERT model to short links and congested conditions., in: 20th  
896 International Transport and Air Pollution Conference 2014. 18-19 September 2014. Graz.  
897 Austria.

898 Samaras, C., Tsokolis, D., Toffolo, S., Magra, G., Ntziachristos, L., Samaras, Z., 2017. Improving fuel  
899 consumption and CO2emissions calculations in urban areas by coupling a dynamic micro  
900 traffic model with an instantaneous emissions model. *Transp. Res. Part D Transp. Environ.*  
901 <https://doi.org/10.1016/j.trd.2017.10.016>

902 Vieira da Rocha, T., Can, A., Parzani, C., Jeanneret, B., Trigui, R., Leclercq, L., 2013. Are vehicle  
903 trajectories simulated by dynamic traffic models relevant for estimating fuel consumption?  
904 *Transp. Res. Part D Transp. Environ.* 24, 17–26. <https://doi.org/10.1016/j.trd.2013.03.012>

905 Wardrop, J.G., 1952. Some Theoretical Aspects of Road Traffic Research, in: *Proceedings of the*  
906 *Institute of Civil Engineers*, Vol. 1-2. pp. 325–378.

907 WHO, 2013. Review of evidence on health aspects of air pollution – REVIHAAP Project.

908 York Bigazzi, A., Rouleau, M., 2017. Can traffic management strategies improve urban air quality?  
909 A review of the evidence. *J. Transp. Heal.* 7, 111–124.  
910 <https://doi.org/10.1016/j.jth.2017.08.001>

911 Zallinger, 2009. Evaluation of a coupled microscopic traffic simulator and instantaneous emission  
912 model. *J. Chem. Inf. Model.* 53, 1689–1699.  
913 <https://doi.org/10.1017/CBO9781107415324.004>

914